Available online at www.sciencedirect.com
SCIENCE DIRECT
Journal of Solid State Chemistry 179 (2006) 2290–2297
JOURNAL OF SOLID STATE CHEMISTRY
www.elsevier.com/locate/jssc

On the distribution of tetrelide atoms (Si, Ge) in $Gd_5(Si_xGe_{1-x})_4$

Sumohan Misra, Gordon J. Miller*

Department of Chemistry and Ames Laboratory, US Department of Energy, Iowa State University, Ames, IA 50011, USA

Received 3 February 2006; received in revised form 1 March 2006; accepted 3 March 2006
Dedicated to Prof. H.G. von Schnering on the 75th anniversary of his birthday
Available online 10 March 2006

Abstract

A crystallographic study of the Si/Ge site preferences in the Si-rich regime of $Gd_5(Si_xGe_{1-x})_4$ and a crystal chemical analysis of these site preferences for the entire range is presented. The room temperature crystal structure of Gd_5Si_4 as well as four pseudobinary phases, $Gd_5(Si_xGe_{1-x})_4$ for $x \geqslant 0.6$, is reported. All structures are orthorhombic (space group *Pnma*), Gd_5Si_4-type and show decreasing volume as the Si concentration increases. Refinements of the site occupancies for the three crystallographic sites for Si/Ge atoms in the asymmetric unit reveal a nonrandom, but still incompletely ordered arrangement of Si and Ge atoms. The distribution of Si and Ge atoms at each site impacts the fractions of possible homonuclear and heteronuclear Si–Si, Si–Ge and Ge–Ge dimers in the various structures. This distribution correlates with the observed room temperature crystal structures for the entire series of $Gd_5(Si_xGe_{1-x})_4$.

Keywords: Gadolinium–germanide–silicide; Coloring problem

1. Introduction

There has been a renaissance in the $RE_5(Si_xGe_{1-x})_4$ systems during the past decade due to discovery of a giant magnetocaloric effect (MCE) in $Gd_5Si_2Ge_2$ [1–7] and extraordinary magnetic responses exhibited by many examples [8–15]. Most of the effort has emphasized the $Gd_5(Si_xGe_{1-x})_4$ system because not only was this the first system to show extraordinary behavior, but the orbitally nondegenerate ground state of the Gd atom eliminates orbital contributions to the local magnetic moment. Numerous experimental and theoretical investigations indicate that the giant MCE is associated with a first-order magnetic transition [16,17], which typically means a structural transition accompanying the change in magnetic order, although the two transitions need not be intrinsically coupled, as seen, e.g., in Er_5Si_4 [18]. It is often observed that changes in magnetic structure also show magnetostriction, but the structural transitions in $Gd_5(Si_xGe_{1-x})_4$ involve changes in crystal symmetry by making or breaking main group-main group chemical bonds.

$Gd_5(Si_xGe_{1-x})_4$ shows two remarkable changes for their room-temperature structures as the Si content varies, shown in Fig. 1. At low Si concentrations ($x \leqslant 0.30$; Ge-rich phases), the orthorhombic Sm_5Ge_4 structure type (O(II)-type) exists [19]; at high Si concentrations ($x \geqslant 0.56$; Si-rich phases), the orthorhombic Gd_5Si_4 structure type (O(I)-type) occurs [20]. At intermediate Si compositions, $0.40 \leqslant x \leqslant 0.503$, the monoclinic $Gd_5Si_2Ge_2$ structure (M) type [21], which is a distorted version of either orthorhombic end phase, is found, but appears to be metastable. Heat treatment of samples for $x = 0.50$ at temperatures below 1000 K showed transformation to the O(I)-type structure and partial eutectoidal decomposition into $Gd_5(Si_xGe_{1-x})_3$ and $Gd(Si_xGe_{1-x})$ [22]. Nevertheless, this decomposition occurs slowly and once cooled below ca. 570 K, the monoclinic phase remains. Furthermore, there are two regions, $0.30 < x < 0.40$ and $0.503 < x < 0.56$, where two respective boundary phases are observed [22]. All three structure types are constructed from topologically identical layers that can be stitched together by main group-main group *Tt*–*Tt* bonds (*Tt* = tetrelide element; Si or Ge). In the Sm_5Ge_4-type, these bonds are not really bonds at all: the Ge–Ge separations exceed 3.5 Å; in the Gd_5Si_4-type, the distances fall well within Si–Si single-bonded distances

*Corresponding author. Fax: +1 515 294 0105.
E-mail address: gmiller@iastate.edu (G.J. Miller).

0022-4596/$ - see front matter © 2006 Elsevier Inc. All rights reserved.
doi:10.1016/j.jssc.2006.03.001

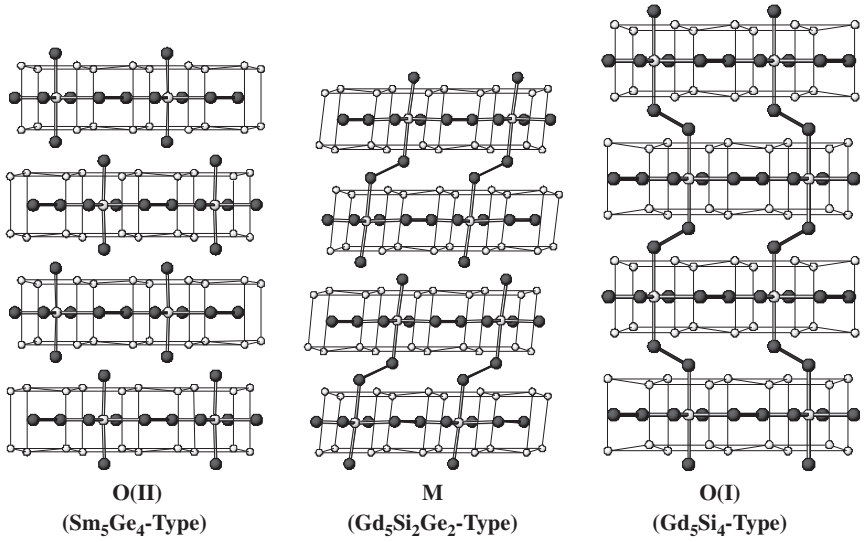

Fig. 1. Projections of the three crystal structures observed for the $Gd_5(Si_xGe_{1-x})_4$ series, which emphasizes the slabs and their interconnections. Shaded circles are Si or Ge sites; larger open circles are Gd3 sites; smaller open circles are Gd1 and Gd2 sites at vertices of the polyhedral frameworks. Lines are drawn to highlight the $[Gd_5(Si_xGe_{1-x})_4]$ slabs as well to emphasize *Tt*–*Tt* and Gd3–*Tt* bonds.

of 2.6 Å. The monoclinic $Gd_5Si_2Ge_2$ shows both types of interactions. These different structures can occur for a given composition by changing temperature or magnetic field, and are at the heart of the giant MCE in $Gd_5Si_2Ge_2$: the monoclinic structure transforms into the O(I)-type at the Curie temperature of 276 K [22].

Previous single crystal X-ray diffraction studies [23] for the Ge-rich phases in the $Gd_5(Si_xGe_{1-x})_4$ system showed that the Si and Ge distributions were not completely random nor completely ordered among the crystallographic sites occupied by these main group elements. This phenomenon could be explained by a competition between enthalpic and entropic factors: enthalpy favors segregation of Si and Ge into the different sites whereas entropy favors mixing, especially with increasing temperature. To obtain a complete characterization of this series and to attempt an understanding of the structural changes, the phase behavior and the physical properties in this system, we have continued these single crystal investigations into the Si-rich region and report these results and conclusions in this paper.

2. Experimental section

2.1. Syntheses

The $Gd_5(Si_xGe_{1-x})_4$ samples, where $x = 0.6$, 0.7, 0.8, 0.9 and 1.0, were prepared by arc-melting its constituent elements in an argon atmosphere on a water-cooled copper hearth. The starting materials were pieces of Gadolinium (99.99 wt%, Materials Preparation Center, Ames Laboratory), Silicon (99.9999 wt%, Alfa Aesar) and Germanium (99.9999 wt%, Alfa Aesar). Each ingot had a total weight of ca. 1.9 g and was remelted several times to ensure homogeneity. Weight losses during melting were less than 0.1 wt%.

2.2. X-ray powder diffraction

The as-cast samples were examined by X-ray powder diffraction for identification and to assess phase purity. Powder patterns were obtained using an Enraf-Nonius Guinier camera using monochromatized Cu*K*α radiation. The purity and homogeneity of all phases was confirmed by comparison of X-ray powder diffraction patterns to those calculated from single-crystal data using the *PowderCell* software [24]. The X-ray powder diffraction patterns for all samples could be completely indexed by orthorhombic Gd_5Si_4-type structures and the refined lattice parameters are listed in Table 1.

2.3. Single-crystal X-ray crystallography

Multiple single crystals from the as-cast samples (without annealing) were mounted on the tip of a glass fiber. To check for possible effects of annealing on the distribution of Si and Ge atoms, the sample with $x = 0.6$ was annealed at 800 °C for 1 week and then room temperature intensity data were collected on a single crystal. The refined composition was $Gd_5Si_{2.39}Ge_{1.61(3)}$, which is in agreement with the refined composition without annealing (see Table 2). The refined occupancy for the T1 site is 0.456(7), for the T2 site is 0.323(10), and for the T3 site is 0.369(10). Room temperature intensity data were collected on a Bruker Smart Apex CCD diffractometer with Mo*K*α radiation ($\lambda = 0.71073$ Å) and a detector-to-crystal distance of 5.990 cm. Data were collected over full spheres of reciprocal space by taking three sets of 606 frames with 0.3° scans in ω with an exposure time of 10 s

Table 1
Lattice parameters for $Gd_5(Si_xGe_{1-x})_4$ ($x \geqslant 0.6$) as obtained by X-ray powder diffraction (space group *Pnma* (No. 62), Cu$K\alpha$ radiation, 2θ range = 4–100°, $T = 273(2)$ K, $Z = 4$)

x	0.6	0.7	0.8	0.9	1.0
Loaded composition (Gd:Si:Ge)	5:2.4:1.6	5:2.8:1.2	5:3.2:0.8	5:3.6:0.4	5:4:0
Refined composition	$Gd_5Si_{2.40}Ge_{1.60(4)}$	$Gd_5Si_{2.79}Ge_{1.21(4)}$	$Gd_5Si_{3.16}Ge_{0.84(4)}$	$Gd_5Si_{3.59}Ge_{0.41(5)}$	Gd_5Si_4
a (Å)	7.514(2)	7.508(2)	7.503(2)	7.500(2)	7.500(3)
b (Å)	14.775(5)	14.777(4)	14.775(4)	14.770(5)	14.756(6)
c (Å)	7.797(2)	7.779(2)	7.767(2)	7.765(3)	7.735(3)
V (Å^3)	865.6(5)	863.0(4)	861.0(4)	860.2(5)	856.0(6)

The refined compositions arise from refinements from single crystal X-ray diffraction.

Table 2
Crystallographic data for $Gd_5(Si_xGe_{1-x})_4$ ($x \geqslant 0.6$) as obtained by single crystal X-ray diffraction (space group *Pnma* (No. 62), Mo$K\alpha$ radiation, 2θ range = 4–57°, $T = 273(2)$ K, $Z = 4$)*

x	0.6	0.7	0.8	0.9	1.0
Refined composition	$Gd_5Si_{2.40}Ge_{1.60(4)}$	$Gd_5Si_{2.79}Ge_{1.21(4)}$	$Gd_5Si_{3.16}Ge_{0.84(4)}$	$Gd_5Si_{3.59}Ge_{0.41(5)}$	Gd_5Si_4
a (Å)	7.507(2)	7.506(2)	7.498(3)	7.494(2)	7.482(2)
b (Å)	14.767(5)	14.789(4)	14.751(5)	14.774(5)	14.738(4)
c (Å)	7.786(3)	7.790(2)	7.784(3)	7.756(2)	7.746(2)
V (Å^3)	863.2(5)	864.7(4)	861.0(5)	858.8(4)	854.2(4)
Independent reflections	1064	1071	1069	1074	1067
No. of parameters	50	50	50	50	47
Final R indices [$I > 2\sigma(I)$]	$R_1 = 0.0372$, $wR_2 = 0.0686$	$R_1 = 0.0432$, $wR_2 = 0.0847$	$R_1 = 0.0341$, $wR_2 = 0.0655$	$R_1 = 0.0452$, $wR_2 = 0.0842$	$R_1 = 0.0326$, $wR_2 = 0.0591$
Peak/hole (e/Å^3)	2.305/−2.272	2.884/−2.849	2.101/−2.597	2.468/−2.462	2.061/−1.898

*Further details of the crystal structure investigation(s) can be obtained from the Fachinformationszentrum Karlsruhe, 76344 Eggenstein-Leopoldshafen, Germany, (fax: (49) 7247-808-666; e-mail: crysdata@fiz.karlsruhe.de) on quoting the depository number CSD 416225, 416226, 416227, 416228 and 416229.

per frame. The ranges of 2θ extended from 4° to 57°. The SMART [25] software was used for data acquisition. Intensities were extracted and then corrected for Lorentz and polarization effects through the SAINT [25] program. Empirical absorption corrections were accomplished with SADABS [25], which is based on modeling a transmission surface by spherical harmonics employing equivalent reflections with $I/\sigma > 3$. Crystallographic data, fractional atomic coordinates and isotropic displacement parameters for all crystals are presented in Tables 2 and 3.

2.4. Electronic structure calculations

Tight-binding, linear muffin-tin orbital (TB-LMTO) electronic band structure calculations in the atomic sphere approximation (ASA) were carried out using the LMTO47 program [26]. Exchange and correlation were treated in a local density approximation. All relativistic effects except spin–orbit coupling were taken into account using a scalar relativistic approximation. The radii of the Wigner–Seitz (WS) spheres were obtained by requiring the overlapping potential to be the best possible approximation to the full potential according to an automatic procedure—no empty spheres were necessary [27]. The WS radii determined by this procedure for the atoms in $Gd_5(Si_xGe_{1-x})_4$ are in the ranges 1.886–2.120 Å for Gd, 1.430–1.442 Å for Si, and 1.440–1.451 Å for Ge. The basis set included Gd 6*s*, 6*p* and 5*d* orbitals, Si 3*s*, 3*p* and 3*d* orbitals, and Ge 4*s*, 4*p* and 4*d* orbitals. The Gd 4*f* orbitals were treated as core wavefunctions occupied by seven valence electrons. Furthermore, the Si 3*d* and Ge 4*d* orbitals were treated by the Löwdin downfolding technique [26]. The *k*-space integrations to determine total energies and densities of states were evaluated by the tetrahedron method using 78 *k*-points in the irreducible wedges of the first Brillouin zones.

3. Results and discussion

The Si-rich region of the $Gd_5(Si_xGe_{1-x})_4$ phase diagram shows a single, orthorhombic Gd_5Si_4 structure type at all temperatures. These phases give a continuous paramagnetic–ferromagnetic transition without change in crystal structure [21]. The surprising issue is that their Curie temperatures exceed that of elemental Gd [19], and increase essentially linearly with increasing Si concentration. This phenomenon is unusual because the Gd atoms are "diluted" by nonmagnetic main group elements and still cannot be explained by appropriate theory. The orthorhombic crystal structure has six atoms in the asymmetric

Table 3
Atomic coordinates, site occupancies and isotropic displacement parameters for $Gd_5(Si_xGe_{1-x})_4$ ($x \geqslant 0.6$) as obtained by single crystal X-ray diffraction

Atom		x	y	z	Occupancy[a]	U_{eq} (Å^2)[b]
$Gd_5Si_{2.40}Ge_{1.60(4)}$						
Gd1	8*d*	0.0237(1)	0.4031(1)	0.1820(1)	1	0.010(1)
Gd2	8*d*	0.6800(1)	0.3775(1)	0.8218(1)	1	0.009(1)
Gd3	4*c*	0.1498(1)	3/4	0.5112(1)	1	0.009(1)
T1	8*d*	0.8469(3)	0.4602(1)	0.5297(2)	0.467(9)	0.012(1)
T2	4*c*	0.0228(4)	3/4	0.1036(4)	0.312(13)	0.010(1)
T3	4*c*	0.2683(4)	3/4	0.8709(4)	0.349(13)	0.008(1)
$Gd_5Si_{2.79}Ge_{1.21(4)}$						
Gd1	8*d*	0.0249(1)	0.4031(1)	0.1823(1)	1	0.011(1)
Gd2	8*d*	0.6810(1)	0.3774(1)	0.8215(1)	1	0.009(1)
Gd3	4*c*	0.1484(1)	3/4	0.5112(1)	1	0.009(1)
T1	8*d*	0.8489(3)	0.4604(2)	0.5291(3)	0.366(9)	0.013(1)
T2	4*c*	0.0222(5)	3/4	0.1028(4)	0.223(12)	0.010(1)
T3	4*c*	0.2666(4)	3/4	0.8724(4)	0.252(12)	0.009(1)
$Gd_5Si_{3.16}Ge_{0.84(4)}$						
Gd1	8*d*	0.0261(1)	0.4030(1)	0.1825(1)	1	0.010(1)
Gd2	8*d*	0.6820(1)	0.3775(1)	0.8211(1)	1	0.008(1)
Gd3	4*c*	0.1470(1)	3/4	0.5113(1)	1	0.008(1)
T1	8*d*	0.8512(3)	0.4603(2)	0.5288(3)	0.247(8)	0.012(1)
T2	4*c*	0.0219(4)	3/4	0.1017(4)	0.165(11)	0.010(1)
T3	4*c*	0.2637(4)	3/4	0.8727(4)	0.177(11)	0.009(1)
$Gd_5Si_{3.59}Ge_{0.41(5)}$						
Gd1	8*d*	0.0279(1)	0.4029(1)	0.1827(1)	1	0.010(1)
Gd2	8*d*	0.6828(1)	0.3776(1)	0.8207(1)	1	0.009(1)
Gd3	4*c*	0.1456(1)	3/4	0.5115(1)	1	0.008(1)
T1	8*d*	0.8538(5)	0.4604(2)	0.5280(5)	0.118(11)	0.010(1)
T2	4*c*	0.0221(7)	3/4	0.1011(7)	0.087(15)	0.011(2)
T3	4*c*	0.2623(7)	3/4	0.8749(7)	0.090(15)	0.011(2)
Gd_5Si_4						
Gd1	8*d*	0.0289(1)	0.4028(1)	0.1827(1)	1	0.009(1)
Gd2	8*d*	0.6837(1)	0.3777(1)	0.8204(1)	1	0.008(1)
Gd3	4*c*	0.1442(1)	3/4	0.5112(1)	1	0.007(1)
T1	8*d*	0.8562(4)	0.4602(2)	0.5281(4)	0	0.010(1)
T2	4*c*	0.0210(5)	3/4	0.0998(5)	0	0.009(1)
T3	4*c*	0.2589(6)	3/4	0.8748(6)	0	0.010(1)

[a]All T1, T2 and T3 sites are fully occupied with a mixture of Ge and Si atoms. Only Ge occupations are listed. The only exception is Gd_5Si_4 where the T1, T2 and T3 sites are fully occupied by Si atoms.
[b]U_{eq} is defined as one-third of the trace of the orthogonalized U_{ij} tensor.

unit: three distinct sites for Gd atoms; and three distinct sites for Si or Ge atoms. Our single crystal diffraction experiments elucidated the distribution of Si and Ge atoms among the three crystallographic sites for these elements. We label these sites as T1 for between slabs and T2, T3 for within slabs. In accord with earlier work on the Ge-rich examples [23], the distributions of Si and Ge atoms are not completely random, nor are they completed ordered. Nevertheless, there is a clear preference for Ge atoms in the T1 sites and for Si atoms in the T2 and T3 sites. Naturally, as the Si concentration increases, all sites become rich in Si atoms.

Now, the diffraction experiment provides a coarse-grained average of atomic distributions over several thousand unit cells and the occupations of various crystallographic sites are based upon independent probability distributions and not conditional probability distributions. Therefore, we can calculate the fractions of allowed homonuclear Si–Si and Ge–Ge and heteronuclear Si–Ge dimers present in these structures for the various compositions by using a binomial distribution, which assumes that no short-range order exists throughout the sample. For example, if the site occupancy factor for Ge at site T1 is u, then the corresponding factor for Si at site T1 is $v = 1 - u$, and we can work out the distribution of Ge–Ge, Ge–Si and Si–Si dimers by $(u + v)^2 = u^2 + 2uv + v^2$. In this expression, u^2 = fraction of Ge–Ge dimers; $2uv$ = fraction of Si–Ge dimers; and v^2 = fraction of Si–Si dimers found at T1–T1 sites throughout the crystal. The Ge site occupancy factors for the T1, T2 and T3 sites as a function of x in $Gd_5(Si_xGe_{1-x})_4$ are plotted in Fig. 2. A completely random distribution of Si and Ge atoms among the sites would produce 3 coincident, linear plots. The graph also indicates the boundaries between the various structural regions.

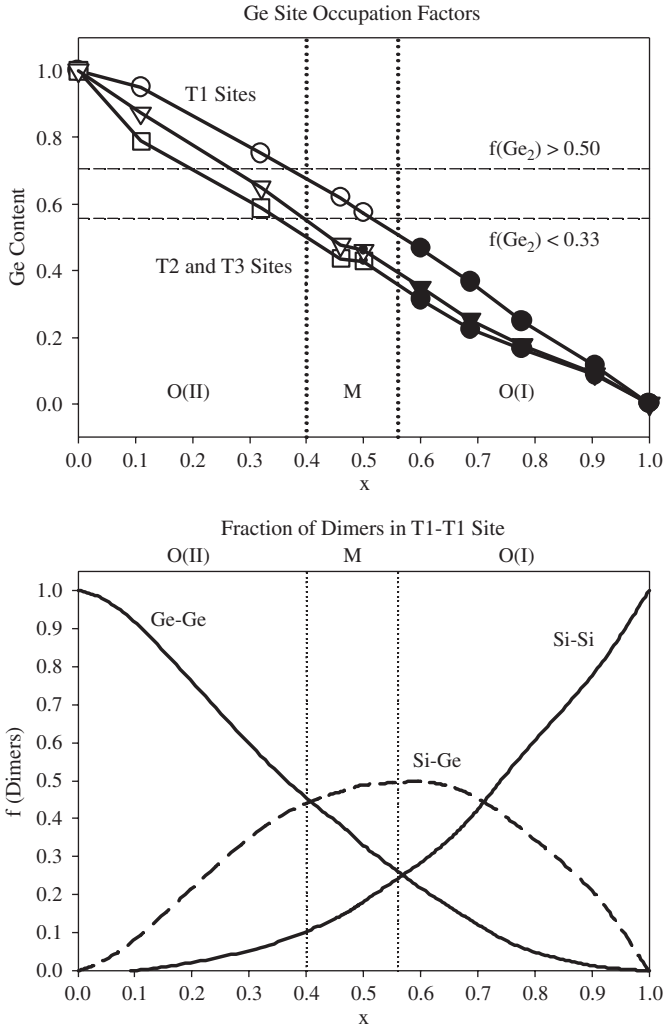

Fig. 2. (Top) Ge occupation in each T site in $Gd_5(Si_xGe_{1-x})_4$ as a function of Si concentration, x. The dark symbols are from this work; the open symbols come from Ref. [23]. The three different structure regimes at room temperature are noted by vertical dotted lines. See text for explanation of the horizontal dashed lines. (Bottom) Fraction of Ge–Ge (solid), Si–Ge (dashed) and Si–Si (solid) dimers at the T1–T1 sites as a function of Si concentration, x.

Note that the Gd_5Si_4-type structure with short T1–T1 contacts occurs as long as the fraction of Ge–Ge dimers in these sites is below 33%, which means that the fraction of Ge in the T1 site, $u<57.7\%$. When the fraction of Ge–Ge dimers exceeds 50%, i.e., $u>71.4\%$, then these T1–T1 bonds are completely severed in the room temperature structures. For intermediate concentrations, $57.7\%<u<71.4\%$, the monoclinic structure is observed in which one-half of the T1–T1 contacts are short and one-half of them are long.

From a different perspective, we plot the fractions of Ge–Ge, Si–Ge, and Si–Si dimers that occur at the T1–T1 sites as a function of x. Since there is a preference for Ge atoms in the T1 sites, these graphs are skewed away from the midpoint, $x=1/2$. According to the graph, in the range $0\leqslant x\leqslant 0.4$, Ge–Ge dimers are most abundant; from $0.4\leqslant x\leqslant 0.7$, Si–Ge dimers dominate; and then for $0.7\leqslant x\leqslant 1.0$, Si–Si dimers are most abundant. Furthermore, the fraction of Si–Si dimers exceeds that of Ge–Ge dimers for $x\geqslant 0.56$. We, therefore, see a correlation between the observed room-temperature structure in the $Gd_5(Si_xGe_{1-x})_4$ series and the distribution of Si and Ge atoms at the T1 positions. The O(II) structure, with no T1–T1 bonds, exists when the concentration of Ge–Ge dimers is highest; the O(I) structure, with all T1–T1 bonds, occurs when the concentration of Si–Si dimers exceeds that of the Ge–Ge dimers. The monoclinic M structure exists for intermediate values. In our opinion, size arguments cannot provide the entire rationale for the distinctive changes in interatomic T1–T1 distances with composition. Nevertheless, the effects of size are clearly seen in trends in unit cell volumes with x. Using volume increments for zero valent Si and Ge from Biltz's compendium (19.98 $Å^3$/atom for Si; 22.43 $Å^3$/atom for Ge) [28], one obtains a consistent range of volume increments for Gd (26.5–26.8 $Å^3$/atom) from the observed volumes for $Gd_5(Si_xGe_{1-x})_4$. Furthermore, the trends in T1–T1 and T2–T3 distances that are shown in Fig. 3, show the size effect, but point out the distinct difference in chemical bonding that occurs in these two sets of dimers.

In an earlier paper, we showed that the site preferences for Si and Ge atoms could be explained by a site energy and bond energy argument [23]. The site energy argument concludes that the T1 sites are attractive for the more electronegative element (Ge). The bond energy argument shows that the site symmetry of the T1–T1 contacts allows mixing between σ_p^* and π molecular orbitals of the T1–T1 dimer. Thus, the weaker Ge–Ge bond pair loses less energy by occupying the T1–T1 site than the Si–Si bond pair does. Therefore, these two distinct arguments give consistent predictions, but there are other significant changes in Gd–(Si,Ge) and Gd–Gd interactions as the structure type varies along the $Gd_5(Si_xGe_{1-x})_4$ series. Trends for the various interatomic distances across the entire $Gd_5(Si_xGe_{1-x})_4$ series are illustrated in Fig. 3 (data for Ge-rich samples are taken from Ref. [23]; data for Si-rich samples come from this work). Although the most notable change occurs for the T1–T1 distance along the series O(II)–M–O(I) as x increases, there are also significant distance variations associated with the Gd1 sites. The graphs of distances show clear trends, with some irregularities among the monoclinic structures, which can be attributed to the occurrence of merohedral twins in all cases and the inherent difficulties to obtain well-resolved parameters for such samples [16]. Nevertheless, as the T1–T1 distance decreases sharply from the O(II) to the O(I) structure, there is a distinct switch in length between two T1–Gd1 contacts. Fig. 4 illustrates the coordination environments for the T1 sites in both the O(I) and O(II) structures to highlight these changes. In both cases the T1 atom is surrounded by a tricapped trigonal prism: the prism is formed by six Gd atoms while the capping atoms are another T1 site, one Gd3 site, and another Gd1 site.

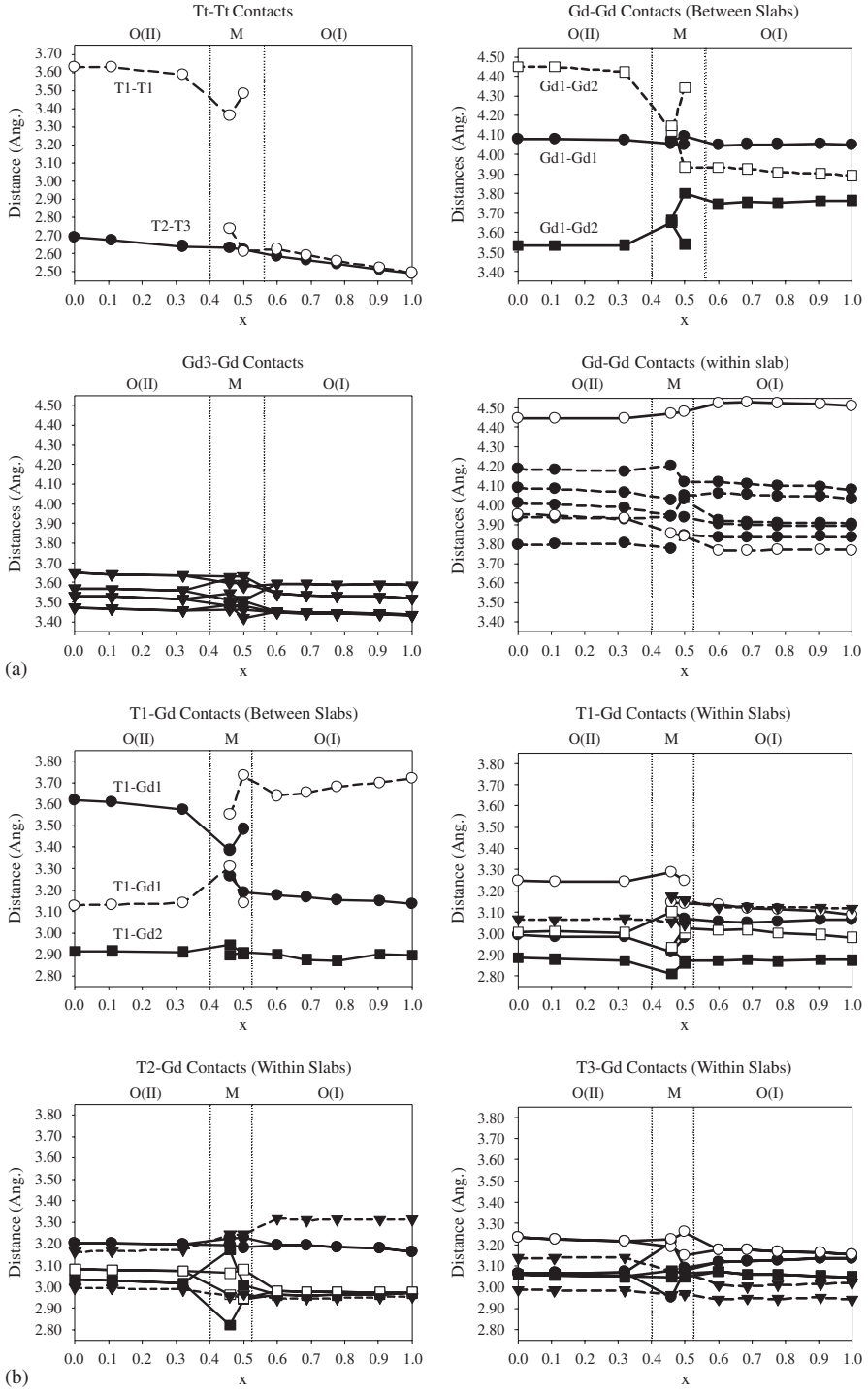

Fig. 3. (a) Interatomic distance variations in $Gd_5(Si_xGe_{1-x})_4$ as a function of Si concentration, x. These graphs illustrate trends in *Tt–Tt* and Gd–Gd distances. The distance scale on all Gd–Gd graphs are identical to illustrate the relative magnitudes. (b) Interatomic distance variations in $Gd_5(Si_xGe_{1-x})_4$ as a function of Si concentration, x. These graphs illustrate trends in *Tt*–Gd distances. The distance scale on all *Tt*–Gd graphs are identical to illustrate the relative magnitudes.

In the O(I) structure, with the short T1–T1 contact (ca. 2.49 Å), the T1–Gd1 contact capping the trigonal prism is long (ca. 3.73 Å). In the O(II) structure, the corresponding T1–Gd1 contact has decreased to 3.13 Å while the T1–T1 distance is now ca. 3.63 Å. Note in the figure that one of the T1–Gd1 distances within the trigonal prism also increases from ca. 3.14 to 3.62 Å as the structure switches from O(I)-type to O(II)-type.

The other significant change arises for Gd–Gd interslab distances: in the O(II) structure, there is a short Gd1–Gd1 contact (ca. 3.53 Å) that expands to ca. 3.76 Å in the O(I) structure type (Fig. 5). Thus, we can simply state that

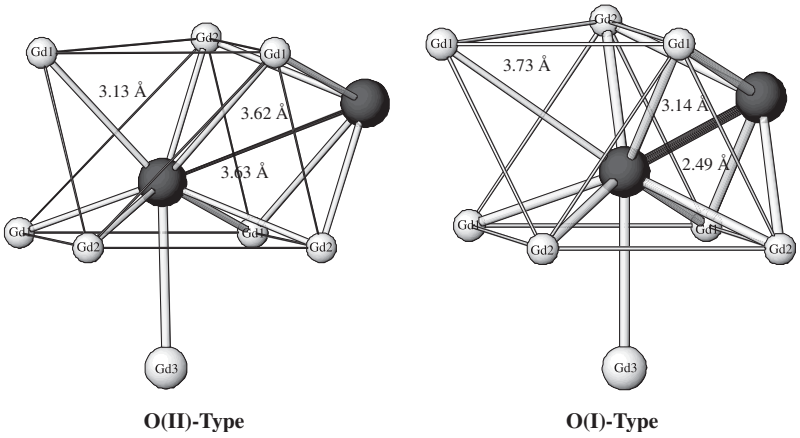

Fig. 4. Coordination environments surrounding the T1 sites in the orthorhombic O(II) and O(I) structures. Interatomic distances showing significant differences between the structures are included.

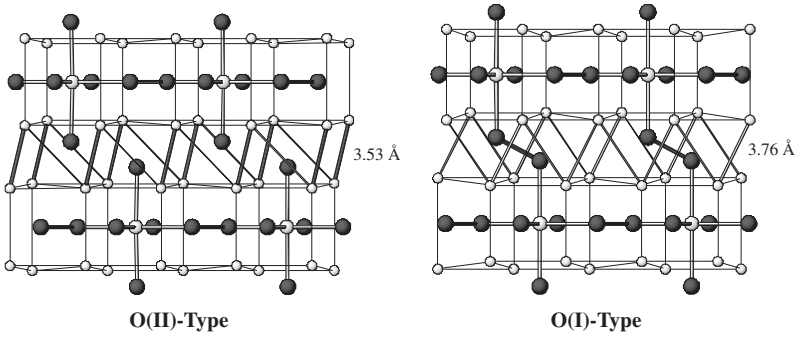

Fig. 5. Interslab contacts for the O(II) and O(I) structure types.

Tt–*Tt* bonds in the O(I) structure are exchanged for *Tt*–Gd and Gd–Gd bonds in the O(II) structure. In Gd_5Ge_4, these short Gd–Gd bonds were used to explain the observed metal-semiconductor transition at 110 K [29], and they can also help explain the antiferromagnetic ordering observed for the low-temperature O(II) phases in the Ge-rich $Gd_5(Si_xGe_{1-x})_4$. In general, however, the shortest Gd–Gd distances in these structures are found between Gd3 and Gd1/Gd2 atoms (the pseudo-cubic coordination sphere)—see Fig. 3.

As a final comment about the variations in interatomic distances shown in Fig. 3, many experimental and theoretical discussions concerning this $Gd_5(Si_xGe_{1-x})_4$ series rely on the slabs remaining intact. This distance analysis essentially confirms this picture, although there are some subtle distance rearrangements across the series. Nevertheless, changes in these interatomic contacts are not as noticeable as those changes occurring between slabs.

Completing this structural analysis and distribution of Si and Ge atoms in the $Gd_5(Si_xGe_{1-x})_4$ series of structures sheds further light on the importance of chemical bonding factors influencing their structures and physical properties. The changes in crystal structure, which can be driven by temperature, magnetic field and temperature, as well as by chemical substitutions, occur due to the subtle differences in chemical bonding strengths. Electronic structure calculations using the TB-LMTO–ASA approach on different arrangements of Si and Ge atoms distributed among the T1, T2 and T3 sites consistently give lower energies to those arrangements where Ge occupies the T1 sites [23]. As part of this study, we explored the total electronic energy differences for $Gd_5Si_2Ge_2$ in the three different structure types: O(I), M and O(II) and for two distinct arrangements of Si and Ge atoms: (i) Ge in T1, Si in T2 and T3; or (ii) Si in T1, Ge in T2 and T3. These results are summarized in Table 4. In all cases, Ge atoms prefer the T1 sites, but the energy differences increase from O(I)-type to M-type to O(II)-type: ca. 0.02 eV/formula unit for O(I); ca. 0.11 eV/

Table 4
Summary of relative total energies calculated for various models of Gd_5Ge_4, $Gd_5Si_2Ge_2$ and Gd_5Si_4 by TB-LMTO–ASA

Model	Gd_5Ge_4	$Gd_5Si_2Ge_2$	Gd_5Si_4
O(I):Ge in T1	0.000	0.000	—
O(I):Si in T1	—	0.027	0.000
M:Ge in T1	0.043	0.097	—
M:Si in T1	—	0.205	0.242
O(II):Ge in T1	0.177	0.250	—
O(II):Si in T1	—	0.420	0.437

All energies are given in units of eV/formula unit, and are expressed relative to the lowest energy arrangement for each composition.

formula unit for M; and ca. 0.17 eV/formula unit for O(II). Thus, there is a greater tendency for Si and Ge mixing for the O(I)-type structures with short T1–T1 contacts. We also examined the relative total energies for Gd_5Si_4, $Gd_5Si_2Ge_2$ and Gd_5Ge_4 in the three structure types. For these calculations, hypothetical structures were necessary in which the unit cell volumes were held constant for a given composition while the structural parameters were scaled isotropically to maintain constant relative distances and angles. As Table 4 indicates, for the entire series, the calculated ground state structure of $Gd_5(Si_xGe_{1-x})_4$ is the orthorhombic O(I)-type, which agrees with earlier calculations [30]. The orthorhombic O(II)-type is more competitive with Ge-rich examples, as is observed experimentally, and its calculated total electronic energy increases relative to the O(I)-type with increasing Si concentration. The monoclinic phase lies intermediate in energy between the O(I) and O(II)-type structures—note that earlier calculations [30] found the monoclinic phase to be lower in energy than the O(I)-type but for a smaller monoclinic angle than the experimentally determined one (ca. 91.7° vs. 93.2°). Nevertheless, the computational results allow us to conclude that there is a strong correlation between the occupation of the T1 sites and the observed structures or possible phase behavior of $Gd_5(Si_xGe_{1-x})_4$. Further efforts to clarify these models for other rare-earth systems are underway.

4. Summary

The distribution of Si and Ge atoms among the various *Tt* sites in the $Gd_5(Si_xGe_{1-x})_4$ series has been completed by single crystal X-ray diffraction experiments. With the results from Ref. [23], we see a clear correlation between the distribution of Si and Ge atoms at the T1 sites between the slabs and the nature of the T1–T1 contacts at room temperature. A thorough analysis of the interatomic distances for the series indicated significant changes in some T1–Gd and Gd–Gd interactions between slabs as the structure varies, and these variations can have significant effects on their physical properties. Electronic structure calculations provide a rationale for these observations, but still do not give a clear understanding of the complex phase behavior in these compounds.

Acknowledgments

The authors thank Prof. Yurij Mozharivskyj for informative discussions. This work was carried out at the Ames Laboratory, which is operated for the US Department of Energy by Iowa State University under Contract No. W-7405-ENG-82. This work was supported by the Materials Sciences Division of the Office of Basic Energy Sciences of the US Department of Energy.

References

[1] V.K. Pecharsky, K.A. Gschneidner Jr., Phys. Rev. B 78 (1997) 4494.
[2] V.K. Pecharsky, K.A. Gschneidner Jr., Appl. Phys. Lett. 70 (1997) 3299.
[3] V.K. Pecharsky, K.A. Gschneidner Jr., J. Magn. Magn. Mater. 167 (1997) L179.
[4] A. Giguere, M. Foldeaki, R. Ravi Gopal, T.K. Bose, A. Frydman, Phys. Rev. Lett. 83 (1999) 2262.
[5] K.A. Gschneidner Jr., V.K. Pecharsky, H.G.M. Duijin, E.M. Levin, Phys. Rev. Lett. 85 (2000) 4190.
[6] A.O. Pecharsky, K.A. Gschneidner Jr., V.K. Pecharsky, J. Appl. Phys. 93 (2003) 4722.
[7] K.A. Gschneidner Jr., V.K. Pecharsky, A.O. Tsokol, Rep. Prog. Phys. 68 (2005) 1479.
[8] L. Morellon, J. Blasco, P.A. Algarabel, M.R. Ibara, Phys. Rev. B 62 (2000) 1022.
[9] L. Morellon, P.A. Algarabel, M.R. Ibarra, J. Blasco, B. Garcia-Landa, Phys. Rev. B 58 (1998) R14721.
[10] C. Magen, L. Morellon, P.A. Algarabel, C. Marquina, M.R. Ibara, J. Phys.: Condens. Matter 15 (2003) 2389.
[11] L. Morellon, J. Stankiewicz, B. Garcia-Landa, P.A. Algarabel, M.R. Ibarra, Appl. Phys. Lett. 73 (1998) 3462.
[12] E.M. Levin, V.K. Pecharsky, K.A. Gschneidner Jr., Phys. Rev. B 60 (1999) 7993.
[13] E.M. Levin, V.K. Pecharsky, K.A. Gschneidner Jr., J. Magn. Magn. Mater. 210 (2000) 181.
[14] E.M. Levin, V.K. Pecharsky, K.A. Gschneidner Jr., Phys. Rev. B 63 (2001) 174110.
[15] J. Stankiewicz, L. Morellon, P.A. Algarabel, M.R. Ibarra, Phys. Rev. B 61 (2000) 12651.
[16] W. Choe, V.K. Pecharsky, A.O. Pecharsky, K.A. Gschneidner Jr., V.G. Young Jr., G.J. Miller, Phys. Rev. Lett. 84 (2000) 4617.
[17] W. Choe, G.J. Miller, J. Meyers, S. Chumbley, A.O. Pecharsky, Chem. Mater. 15 (2003) 1413.
[18] Y. Mozharivskyj, A.O. Pecharsky, V.K. Pecharsky, G.J. Miller, K.A. Gschneidner Jr., Phys. Rev. B 69 (2004) 144102.
[19] F. Holtzberg, R.J. Gambino, T.R. McGuire, J. Phys. Chem. Solids 28 (1967) 2283.
[20] G.S. Smith, Q. Johnson, A.G. Tharp, Acta Crystallogr. 22 (1967) 269.
[21] V.K. Pecharsky, K.A. Gschneidner Jr., J. Alloys Compd. 260 (1997) 98.
[22] A.O. Pecharsky, K.A. Gschneidner Jr., V.K. Pecharsky, C.E. Schindler, J. Alloys Compd. 338 (2002) 126.
[23] W. Choe, A.O. Pecharsky, M. Wörle, G.J. Miller, Inorg. Chem. 42 (2003) 8223.
[24] W. Kraus, G. Nolze, Powder Cell for Windows, Version 2.4, 2000.
[25] XRD Single Crystal Software, Bruker Analytical X-ray Systems, Madison, USA, 2002.
[26] (a) O.K. Andersen, Phys. Rev. B 12 (1975) 3060;
(b) O.K. Andersen, O. Jepsen, Phys. Rev. Lett. 53 (1984) 2571;
(c) O.K. Andersen, O. Jepsen, D. Glötzel, in: F. Bassani, F. Fumi, M.P. Tosi (Eds.), Highlights of Condensed-Matter Theory, North-Holland, New York, 1985;
(d) O.K. Andersen, Phys. Rev. B 34 (1986) 2439.
[27] O. Jepsen, O.K. Andersen, Z. Phys. B 97 (1995) 35.
[28] (a) W. Biltz, Raumchemie der festen Stoffe, Verlag von Leopold Voss, Leipzig, 1934;
(b) R. Dronskowski, Computational Chemistry of Solid State Materials, Wiley-VCH, Weinheim, 2005.
[29] E.M. Levin, V.K. Pecharsky, K.A. Gschneidner Jr., G.J. Miller, Phys. Rev. B 64 (2001) 235103.
[30] V.K. Pecharsky, G.D. Samolyuk, V.P. Antropov, A.O. Pecharsky, K.A. Gschneidner Jr., J. Solid State Chem. 171 (2003) 57.